International Journal on Recent and Innovation Trends in Computing and Communication
ISSN: 2321-8169 Volume: 11 Issue: 7s
DOI: https://doi.org/10.17762/ijritcc.v11i7s.7021
***Article Received**: 02 April 2023 **Revised:** 24 May 2023 **Accepted:** 09 June 2023*

Newton's Law of Gravitational Force (NLGF) based Machine Learning Technique for Uneven Illuminated Face Detection

M. Shalima Sulthana[1], C. Naga Raju[2]
[1]Research Scholar
m.s.sulthana2012@gmail.com
Department of Computer Science and Engineering
YSR Engineering College of YVU
Yogivemana University- Kadapa
[2]Professor
Department of Computer Science and Engineering
YSR Engineering College of YVU
Yogivemana University- Kadapa

Abstract— A photo gallery is crucial for organizing your photos, presenting them in beautiful categories, and doing sophisticated memory searches. The photo gallery is portrayed in a vocabulary of nonlinear similarities to the prototype face image collection. One of the difficult research ideas for machine learning technologies is the maintenance of a photo gallery using facial recognition. Based on changes in the faces' appearance, faces are identified. This research proposes novel machine learning algorithms to recognize faces by characterizing the majority of discriminating local characteristics, which maximizes the dissimilarity between face photos of different persons and reduces the dissimilarity between features between face images of the same person. This method relies on Newton's third law of gravitational force to determine the relationship between pixels to extract the features of noisy accurately and efficiently, unevenly illuminated, and rotationally invariant face images.

Keywords- NLGF, ENLGF, Gravitational Force, Face recognition, Gamma-correction.

I. INTRODUCTION

Face recognition is a popular research area, On account of its extraordinary success and vast social applications. Every human face in this world has the same facial features like eyes, ears, lips and nose, etc. however, every face shows different structures. Several facial recognition algorithms have been proposed during the last few decades, such as Bayesian facial recognition [1], facial recognition with support vector machines [2], and Eigenfaces [3], However, the images that are obtained in good environments were used to test these algorithms in the past, but failed to show the best results on illumination invariant images. To solve this illumination invariant problem, several existing methods have been applied, including method1: in this method face images are intended to decrease the intensity first, the fundamental techniques come under this method includes gamma-correction [4], logarithmic modification [5], and further advanced methods are proposed to measure this intensity i.e., histogram equalization [6], etc. Method2: modeling strategies are used to detect facial images in various illumination situations i.e., 3Dimentional texture of a human face, in [7] explains the 3Dimentional structure of human faces with various levels of illumination conditions. Method3: invariant feature method, this method is used to detect static features such as edge mapping, Gabor filter and image stabilization of illuminated images. All these approaches reflect the common assumption that wavelengths they produce from all radiational sources are the same. Every image descriptor provides an explicit description of features such as shape, color, texture, or movement that is visible in the images or algorithms or videos. These image descriptors are divided into global descriptors and local descriptors. Global-descriptors are used to describe the texture of an image and color of an image, these global descriptors are outmoded due to their inconsistent performance in the form of illumination and occlusion images [8]. Local descriptors are traditionally categorized as data-driven descriptors, used to enhance the local performance of an image and handcrafted descriptors used to characterize an image local-patches [9] i.e., the key points in the image. Data driven descriptors have been designed and structured in accordance with training data. To identify the optimal configuration in the descriptor parameter space [11] or to generate reduced dimensional binary descriptors [10], training is necessary. Hand-crafted descriptors of an image: SIFT [12] it is used to find local features or major points in an image and Gaussian function is used to calculate scale space, SURF [13] Speed Up

International Journal on Recent and Innovation Trends in Computing and Communication
ISSN: 2321-8169 Volume: 11 Issue: 7s
DOI: https://doi.org/10.17762/ijritcc.v11i7s.7021
***Article Received**: 02 April 2023 **Revised:** 24 May 2023 **Accepted:** 09 June 2023*

Robust Feature gives description of unique features in an image like corner points, spot-points, edge-points, DAISY [14] primarily designed for solid calculations, but dense descriptions produce unwanted and non-informative details [15] and LBP [16] Local Binary Pattern used for texture classification. Local descriptors are conventionally used to compare sparse pixels that are feature points [17]. These reference [18] feature points are utilized as anchors to compute the whole reconstruction. Deep descriptors have recently become available to enable the expanding availability of enormous data sets [19]. Discriminability, matching speed, and memory storage are the three main characteristics used to describe descriptor performance [20]. Feature based image recognition is gaining great popularity because of its robustness, flexibility and used in wide range of applications. Calculating a feature point is said to be best when it can be found quickly and easily, because the feature is important in a good place to compare the next features.

For consistent feature extraction, several properties have been employed, including rigidity, immutability, repetition, and efficiency [21]. Two straight lines crossing at a point, such as a "L," "X," "T," or "high curvature point" in the contour, are considered corner features in an image. Corner response may be computed using corner feature detection, and this response can then be compared to picture edges or less distinguishable regions. Corner points have been found using a variety of approaches, including gradient, intensity, and contour curvature-based [22][23]. The interest points notion for identifying the best feature points was presented by the first automated gradient-based corner recognition algorithm [24]. This technique looks for feature points when the minimum intensity variation of each pixel exceeds a predetermined threshold in eight different directions. Corner detection of meth using intensity SUSAN [25] The "Small Univalue Segment Assimilating Nucleus" algorithm operates by comparing the brightness of the nucleus and a small radius area pixel. Using contours, edges, and salient areas, the curvature-based corner recognition approach obtains corner characteristics [26]. Face feature key points identification has been done over the past several decades using classical learning-based approaches including Support-Vector-Machines (SVM), and decision trees, other classifiers [27][28].FAST is the first approach for matchable point recognition that is based on classic learning [29]. The fundamental principle of feature point identification is to set them apart from other points through the response value, which is utilized to address two issues: I creating discriminatory patterns in an image; and (ii) recognizing prominent features under various situations and picture characteristics [30]. The suggested approach would recognize unevenly lighted, rotation-invariant, and noisy face photos with cheap computing cost and good accuracy rate. Lately, face recognition with machine learning techniques has gained significant popularity [31][32].

II. Problem Formulation

The mass and intensity of each pixel in a picture are equivalent to planetary bodies. Any two items will be drawn to one another due to the phenomenon known as gravity. According to Newton's third law of gravity, every pair of mass-containing objects in the universe is attracted to one another by a gravitational force whose strength is inversely proportional to the sum of the masses of the two objects and independent of their distance from one another.

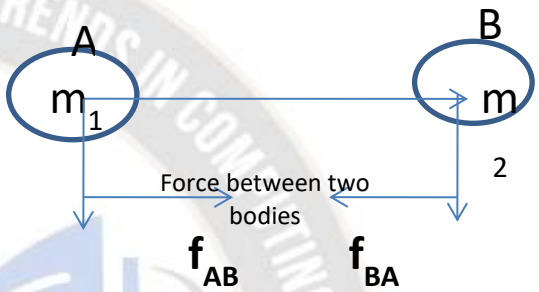

Fig: (1) represents gravitational force of A and B objects

An action and reaction pair, or an application of equal but opposing forces,

causes two bodies, A and B, to experience gravitational pull. In Fig. 1, f_{AB} stands for the force exerted on Body A by Body B, and f_{BA} stands for the opposing force.

$$f_{AB} = - f_{BA} \quad (1)$$

$$f \alpha m_1 \times m_2 \quad (2)$$

$$f \alpha \frac{1}{r2} \quad (3)$$

The gravitational force between two objects at distance d and masses m1 and m2 is described by (f_{AB})

$$f_{AB} = G\frac{m1 \times m2}{d2} \quad (4)$$

Here, the constant G stands for gravity.

Here, angle is Θ used in conjunction with force fAB with regard to the X axis to extract image edges.

International Journal on Recent and Innovation Trends in Computing and Communication
ISSN: 2321-8169 Volume: 11 Issue: 7s
DOI: https://doi.org/10.17762/ijritcc.v11i7s.7021
***Article Received**: 02 April 2023 **Revised:** 24 May 2023 **Accepted:** 09 June 2023*

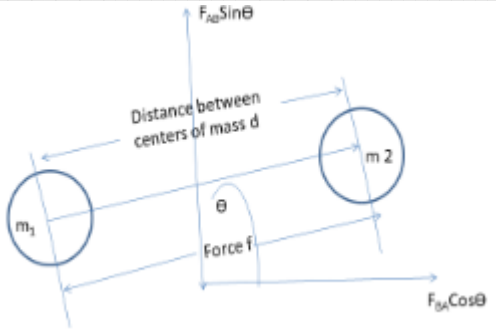

Fig 2: gravitational force with respect to x and y axis between two bodies

Now let's look about the pixels that surround each and every neighborhood pixel of the image's central pixel. The GF (f), which is taken from each pixel in a picture using the x and y axes, is computed as

$$f_x=\sum_{q=1}^{m}(GF\ X\ \frac{Ib\ x\ Ii}{d2mi}\ X\ \cos\Theta\ mi) \quad (5)$$

$$f_y=\sum_{q=1}^{m}(GF\ X\ \frac{Ib\ x\ Ii}{d2mi}\ X\ \sin\Theta\ mi)$$

Here, m stands for the number of adjacent pixels. I_b and I_c represent the center pixel's intensity values, while d^2 m_i is the Euclidean distance between the central pixel and its i^{th} index neighbor. The angle between the center pixel and the x axis is represented by the symbol Θm_i.

It is challenging to compute force when the center pixel intensity value is zero, however this issue may be fixed by changing grey-scale values from 0-255 to 1-255.

The total force magnitude f_{magni} acting on the center pixel is determined as follows: where each force is represented by its direction and magnitude.

$$F_{magni}=\sqrt{(fx)^2+(fy)^2} \quad (6)$$

$$=I_bX\ G\sqrt{\sum_{j=1}^{k}(\frac{Ii}{d2mi}\ X\ \cos\Theta\ mi)2+\sum_{j=1}^{k}(G\ X\ \frac{Ib\ x\ Ic}{d2mi}\ X\ \sin\Theta\ mi)2} \quad (7)$$

f_{angle} that is total force direction is calculated as following

$$=\text{arc tan}\ (\frac{fy}{fx})=\text{arc tan}\left[\frac{\sum_{q=1}^{k}(G\ X\frac{Ib\ x\ Ic}{d2mi}\ X\ \sin\Theta mi}{\sum_{q=1}^{k}(G\ X\frac{Ib\ x\ Ic}{d2mi}\ X\ \sin\Theta mi}\right] \quad (8)$$

Here force is represented by its direction and angle.

III. NEWTON'S LAW OF GRAVITATIONAL FORCE (NLGF)

Gravitational forces exerted by eight neighboring pixels on the center pixel (c) in a 3x3 neighborhood are represented in the following figure.

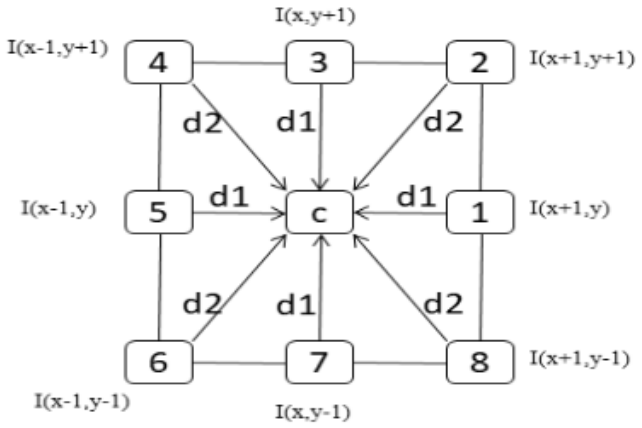

Fig 3: Gravitational forces exerted by eight neighboring pixels on the center pixel (c) in a 3x3 neighborhood.

The Euclidean distance (d) between two pixels with position coordinates of (m, n) and (p, q) is

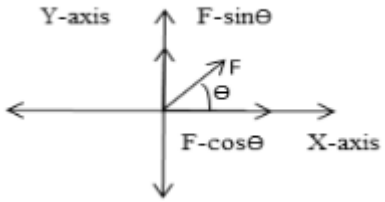

$$d=\sqrt{(m-p)^2+(n-q)^2} \quad (21)$$

In fig 3: The distance between the center pixel and each of its four neighbors in Euclidean space(i.e., directly connected) pixels is denoted by d1.The distance between each of the four diagonally connected pixels and the center pixel is defined in r2.

$$\therefore d_1=1,\ d_2=\sqrt{2} \quad (22)$$

By adding both components (X and Y) of each force separately, the total resulting force acting on the center pixel can be calculated. If a force F acts with respect to the X axis at an angle Θ, then X component (F_x) and Y component (F_y) of that force are $F_x = F_x \cos\Theta$ and $F_y = F_y \sin\Theta$ as shown in fig3.

International Journal on Recent and Innovation Trends in Computing and Communication
ISSN: 2321-8169 Volume: 11 Issue: 7s
DOI: https://doi.org/10.17762/ijritcc.v11i7s.7021
***Article Received**: 02 April 2023 **Revised:** 24 May 2023 **Accepted:** 09 June 2023*

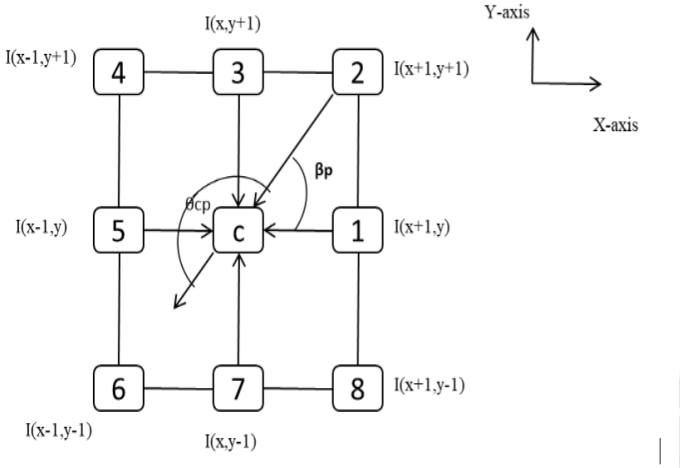

Fig4: The relationship between the positional angle (βp) and the angle of gravitational force (θcp) between two bodies.

The local gravitational force direction on each center pixel inside a 3x3 window is first calculated. In fig 4: a 3x3 window around central pixel is shown where p_i is the index of neighboring pixel and P represents no of neighbors' and ra shows the radius.

By the x and y coordinates p^{th} neighbor pixel represented as (X_p, Y_p).

$$X_p = i_{polate}\left(x + ra * \cos\frac{2\pi x(p-1)}{P}\right) \quad (23)$$

$$Y_p = i_{polate}\left(y - ra * \cos\frac{2\pi x(p-1)}{P}\right) \quad (24)$$

Here p= { 1, 2,3……P) and i_{polate} is interpolation of coordinates.

Here it a 3x3 window so ∴ radius ra=1, no of neighbors P=8, $\frac{2\pi}{P}$ $=45^0$ angle between equally spaced neighbors.

As shown in the fig:4, With respect to x-axis p^{th} pixel $\frac{2\pi x(p-1)}{P}$ positional angle is $\boldsymbol{\beta_p}$ The direction of that force (θcp) with respect to the X axis is computed by adding 180 to the positional angle (p) of the neighboring pixel. As a result, the force exerted by the p-th pixel on the central pixel c at an angle cp is

$$\theta_{cp} = \boldsymbol{\beta_p} + 180^0 = \frac{2\pi x(p-1)}{P} + 180^0 \quad (25)$$

Consider the location angle between c and pixel 2 in Fig. 2. In this case, β2 is 45◦ Fc2 is a force directed from pixel 2 to c. As a result, the angle of force (θc2) with respect to the X axis is $\beta 2 + 180^0 = (45^0 + 180^0) = 225^0$.

By considering 3x3 window around central pixel it's not possible to eliminate the noise from face image completely so 5x5 window around central pixel with gravitational force angle has been proposed.

$$\theta_{cp} = \boldsymbol{\beta_p} + 180^0 = \frac{2\pi x(p-1)}{P} + 180^0 \quad (25)$$

Consider the location angle between c and pixel 2 in Fig. 2. In this case, β2 is 45◦ Fc2 is a force directed from pixel 2 to c. As a result, the angle of force (θc2) with respect to the X axis is $\beta 2 + 180^0 = (45^0 + 180^0) = 225^0$.

By considering 3x3 window around central pixel it's not possible to eliminate the noise from face image completely so 5x5 window around central pixel with gravitational force angle has been proposed.

IV. Extended Newton's Law of Gravitational Force for Face Recognition (ENLGF)

The Extended Newton's Law of Gravitational Force (ENLGF) method detects the face by describing the majority of discriminate local features, which maximizes the dissimilarity between face images of different people and minimizes the similarity between face images of the same person while minimizing noise from detected face images.

Take a look at an image I with a different illumination I (row_i, $colu_i$) an area of A feature of the constant magnitude of the lighting is the original picture intensity of the center pixel and the proportion of a 3X3 neighboring pixels' gravitational forces to those of the center pixel. As illustrated in figure consider a local window (3 × 3) with a center pixel "c". Based on Newton's third universal gravitation law, to the central pixel "c", applying a force on the 8 neighboring pixels. Here "i" represent the index of one pixel. As a result, "Fci" can be used to represent the central pixel (c) force exerted from the i^{th} surrounding pixel. Let the angle between the (c) central pixel and "θ_{ci}" the i^{th} pixel, Then the resulting gravitational force magnitude "F_{mag}" is calculated as

$$F_{mag} = I_e X G X \sqrt{\sum_{p=1}^{m}\left(\frac{Ii}{r2mi} X \cos\theta mi\right)2 + \sum_{j=1}^{k}\left(G X \frac{Ib\,x\,Ie}{r2mi} X \sin\theta mi\right)2} \quad (26)$$

Here, I_e is the intensity value of the center pixel, I_i is the intensity value of the i^{th} neighboring pixel, and r^2m_i is the distance between the central pixel and ith neighboring pixel.

Let square the intensity of central pixel $I_e^{2=} I_e X I_e$.

Therefore, the ratio between force magnitude F_{mag} and I_e^2 denoted as follows

$$ratio = \frac{Fmag}{Ie2}$$

By replacing F_{mag} in (22) by (21) we get

International Journal on Recent and Innovation Trends in Computing and Communication
ISSN: 2321-8169 Volume: 11 Issue: 7s
DOI: https://doi.org/10.17762/ijritcc.v11i7s.7021
***Article Received**: 02 April 2023 **Revised:** 24 May 2023 **Accepted:** 09 June 2023*

$$\text{Ratio}=\frac{Ie\,X\,G\,X\sqrt{\sum_{p=1}^{m}(\frac{Ii}{r2mi}\,X\cos\theta\,mi)2+\sum_{j=1}^{k}(G\,X\frac{Ib\,x\,Ie}{r2mi}\,X\sin\theta mi)2}}{Ie\,X\,Ie} \quad (27)$$

$$\text{If } \frac{Ie}{w}\neq 0 \text{ then, ratio}=\frac{Ie\,X\,G\,X\sqrt{\sum_{p=1}^{m}(\frac{Ii}{r2mi}\,X\cos\theta\,mi)2+\sum_{j=1}^{k}(G\,X\frac{Ib\,x\,Ie}{r2mi}\,X\sin\theta mi)2}}{Ie} \quad (28)$$

$$\text{ratio}=G\,X\sqrt{\frac{\sum_{p=1}^{m}(\frac{Ii}{r2mi}\,X\cos\theta\,mi)2\;)}{Ie}}+\sqrt{\frac{\sum_{p=1}^{m}(\frac{Ii}{r2mi}\,X\cos\theta\,mi)2}{Ie}} \quad (29)$$

Each pixel in an image (I) is represented as the product of two components: R (r_i, c_i), (r_i, c_i) an illumination component and a reflectance component. Horn's illumination-reflection (IRM) model claims (L). It is written as follows:

$$I=Rx\,L \quad (30)$$

Here, it is usually assumed that in a local neighborhood L varies extremely slowly, i.e. L remains relatively constant in a local neighborhood (3x3) while, conversely, R varies significantly. As a result of this theory, we rephrase (2) as follows.

$$\text{ratio}=G\,X\sqrt{\frac{\sum_{p=1}^{m}(\frac{Ii}{r2mi}\,X\cos\theta\,mi)2\;)}{LxIe}}+\sqrt{\frac{\sum_{p=1}^{m}(\frac{Ii}{r2mi}\,X\cos\theta\,mi)2}{LXIe}}$$

$$=G\,X\sqrt{\frac{\sum_{p=1}^{m}(\frac{Ii}{r2mi}\,X\cos\theta\,mi)2\;)}{Ie}}+\sqrt{\frac{\sum_{p=1}^{m}(\frac{Ii}{r2mi}\,X\cos\theta\,mi)2}{Ie}}$$

From Eq (31) we can now see that 'ratio' is the R component and R denotes the intended invariant illumination feature. Thus, the ratio of the exerted resultant gravitational force magnitude by other 3x3 neighborhood pixels is the illumination invariant magnitude to the square of the original picture intensity of the center pixel.

To improve the ratio ('ratio') while reducing noise, we implement the arctan function. As a result, the final ratio is zero; however, a magnitude normalized computation in (3x3) window is calculated as follows:

$$\text{ratio}=\arctan G\,X\left[\sqrt{\frac{\sum_{p=1}^{m}(\frac{Ii}{r2mi}\,X\cos\theta\,mi)2\;)}{Ie}}+\sqrt{\frac{\sum_{p=1}^{m}(\frac{Ii}{r2mi}\,X\cos\theta\,mi)2}{Ie}}\right] \quad (32)$$

It is applied that a set of P pixels in square neighborhood with a length of "(2w+1)".

Here w denotes the distance among the center pixel and the surrounding neighborhoods to a central pixel. (P; w): (8; 1) and (16; 2) two possible combinations of are allowed.

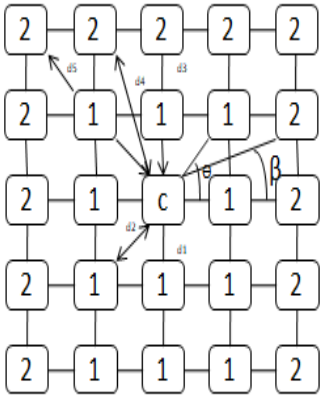

Fig 5: (P; w), i.e. (8; 1) and (16; 2) The pixel distribution with respect to values of P and to the central pixel (c) as well as various directional angles (θ,β) and distances of neighboring pixels (d1,d2,d3,d4,d5).

Depending on distances of neighboring pixels and different positional angles, two distinct linear spatial masks for each single (P; w) combination, as shown in Figure 5 are used.

As a result, four distinct masks are used to determine F_x and F_y using linear spatial filtering. Following are the filter functions:

$$M_X{}^W(x,y)=\begin{cases}\dfrac{\cos(\arctan(\frac{y}{x}))}{x^2+y^2} & x^2+y^2>0\\ 0 & \text{Otherwise}\end{cases} \quad (33)$$

$$M_y{}^W(x,y)=\begin{cases}\dfrac{\sin(\arctan(\frac{y}{x}))}{x^2+y^2} & x^2+y^2>0\\ 0 & \text{Otherwise}\end{cases} \quad (34)$$

$$\text{If } w=1, x\in[-1,0,1] \text{ and } y\in[-1,0,1]; \text{ if } w=2, x\in[-2,-1,0,1,2] \text{ and } y\in[-2,-1,0,1,2].$$

The filters depicted above include some noise resistance. We used the (SNR) signal-to-noise ratio to demonstrate the filters' noise resistance.

Let's say the original image I_0 is a noise-free signal, and we get an image I_n after adding some noise.

Lastly the filter M^w is applied on I_n and an filtered image I_{fi} is generated ∴ I_{fi} represented as follows

$$I_{fi}=I_n * M^w \quad (35)$$

We know that repeating the summing of noisy signals minimizes noise and improves the signal, this process is known as local smoothing.

International Journal on Recent and Innovation Trends in Computing and Communication
ISSN: 2321-8169 Volume: 11 Issue: 7s
DOI: https://doi.org/10.17762/ijritcc.v11i7s.7021
***Article Received**: 02 April 2023 **Revised:** 24 May 2023 **Accepted:** 09 June 2023*

V. FLOW CHART FOR IMPLEMENTATION OF EXTENDED NEWTON'S LAW OF GRAVITATIONAL FORCE FOR FACE RECOGNITION (ENLGF)

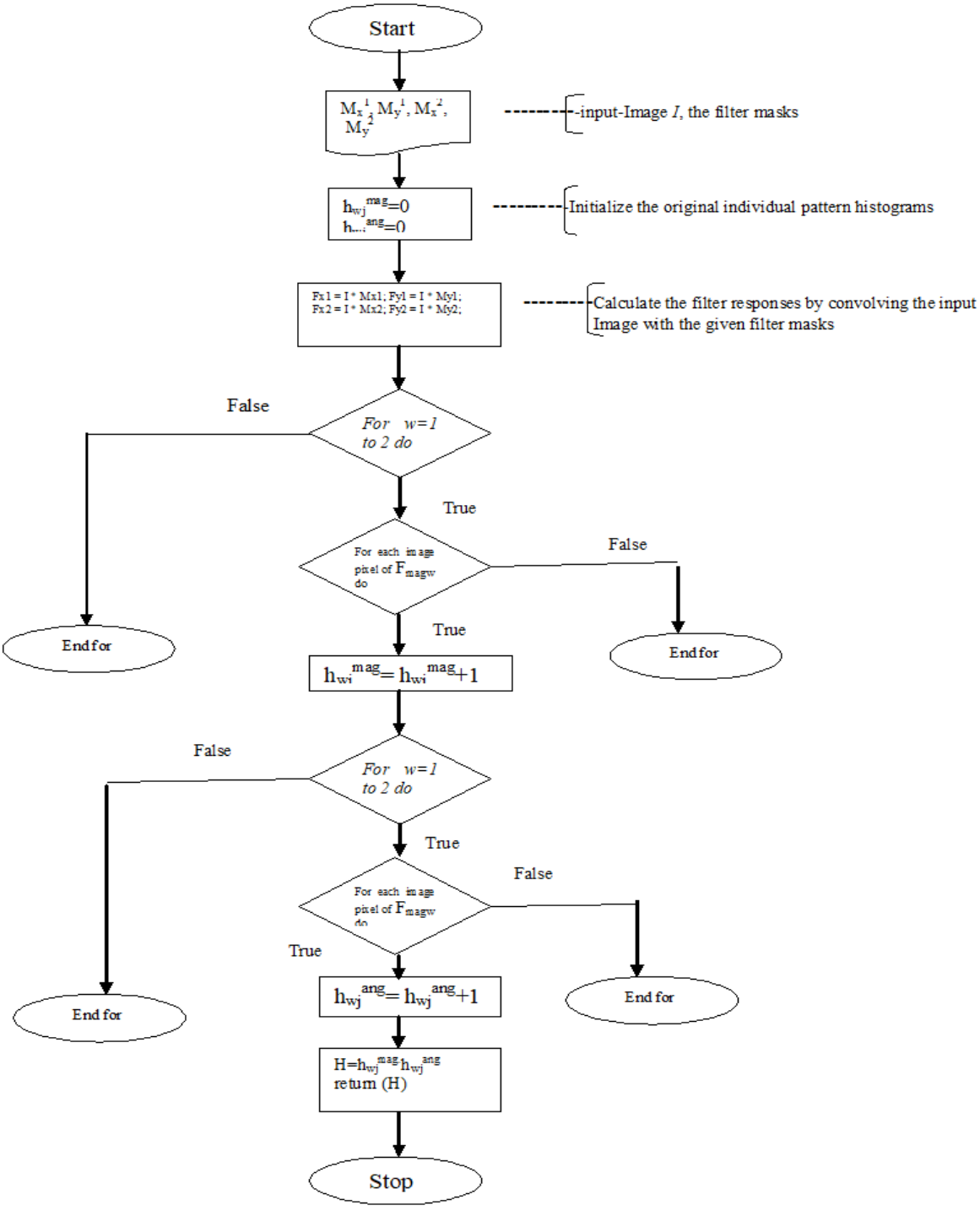

Fig 6: represents the implementation of Extended Newton's Law of Gravitational Force ENLGF.

International Journal on Recent and Innovation Trends in Computing and Communication
ISSN: 2321-8169 Volume: 11 Issue: 7s
DOI: https://doi.org/10.17762/ijritcc.v11i7s.7021
***Article Received**: 02 April 2023 **Revised:** 24 May 2023 **Accepted:** 09 June 2023*

VI. Experimental Results and Discussions

In this investigation, two data sets—YALEB and ORL—for experiments are taken into consideration for evaluating the effectiveness of the ENLGF approach, These Data Sets contains uneven illuminated, rotation invariant and noisy face images. NLGF and ENLGF machine learning techniques are applied on these data sets and confusion matrix is applied to measure the accuracy, precision, and recall, Mean square error (MSE), mean absolute error (MAE), and root mean square error are three statistics that are gathered and used for error detection. (RMSE). For classification we applied several machine learning classifiers like SVM, LR, DTC, RF-Reg, KNN and K-Means classifier.

Support Vector Machine is machine learning technique used to solve regression and classification problems. A model with a linear relationship between the input variables (x) and the only output variable (y) is known as a linear regression. The random forest classifier divides this dataset into subsets'-*means* is an unsupervised classification algorithm. Table 1-Table 4 and Graph1-Graph4 shows accuracy of SVM, LR, RF, and K-MEANS for NLGF and ENLGF methods, it is clearly noticed that the ENLGF technique shows better accuracy than NLGF method. In our proposed methodology, face features are created with both vertical and horizontal lines.fig:7 illustrates extracting vertical features, such as the nose, from the face picture by using dy, and horizontal features, such as the eyes, mouth, and eyebrows, by using dx. We can extract both vertical and horizontal aspects of the face, such as the brows, eyes, lips, and nose, when we combine dy and dx. We can only extract the vertical and horizontal characteristics of a face using dx and dy, but this method is unable to extract the edge regions of an image. As a result, we use gravitational force angle to obtain the corner regions of a face. It is clearly observed that NLGF method fail to reduce the noise. The ENLGF method Using 5x5 window with Local gravitational force angle "θ"accurately and efficiently extracts features from facial photos that are rotated invariant, unevenly lit, and noisy.

result, we use gravitational force angle to obtain the corner regions of a face.

Fig: 7 shows original data base images, horizontal features extracted images, vertical features extracted images, NLGF method, both horizontal and vertical features of ENLGF method and both horizontal and vertical features with angle θ of ENLGF method

International Journal on Recent and Innovation Trends in Computing and Communication
ISSN: 2321-8169 Volume: 11 Issue: 7s
DOI: https://doi.org/10.17762/ijritcc.v11i7s.7021
***Article Received**: 02 April 2023 **Revised:** 24 May 2023 **Accepted:** 09 June 2023*

Accuracy of SVM:

Sample size	NLGF	ENLGF
0.05	0.97	0.98
0.10	0.98	0.99
0.15	0.875	0.875
0.20	0.8181	0.9090
0.25	0.8461	0.9230
0.30	0.875	0.9375
0.35	0.8421	0.8421
0.40	0.7619	0.8095
0.45	0.7916	0.7916
0.50	0.8076	0.8076
0.55	0.75862	0.7931
0.60	0.8125	0.8125
0.65	0.7941	0.7941

Table 1: Accuracy of support vector machine

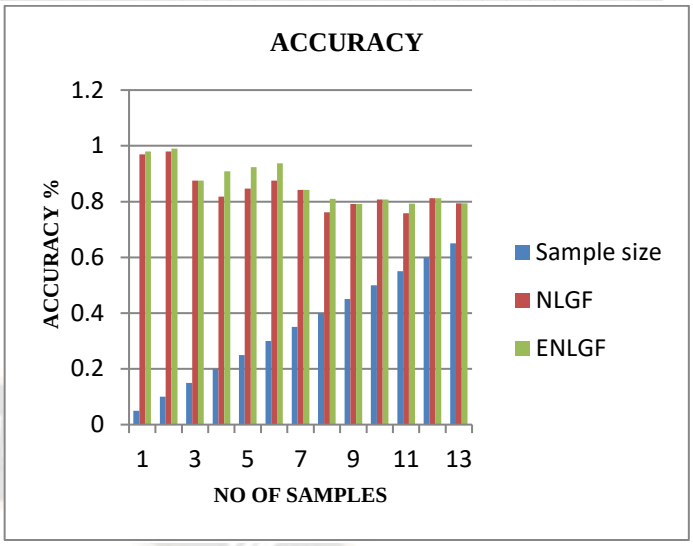

Graph1

LR:

Sample size	NLGF	ENLGF
0.05	0.6666	0.978
0.10	0.8333	0.983
0.15	0.75	0.984
0.20	0.8181	0.995
0.25	0.8461	0.989
0.30	0.875	0.990
0.35	0.7368	0.8947
0.40	0.8095	0.7619
0.45	0.7916	0.7916
0.50	0.7307	0.8076
0.55	0.75862	0.8275
0.60	0.8437	0.8437

Table 2: Accuracy of Linear Regression

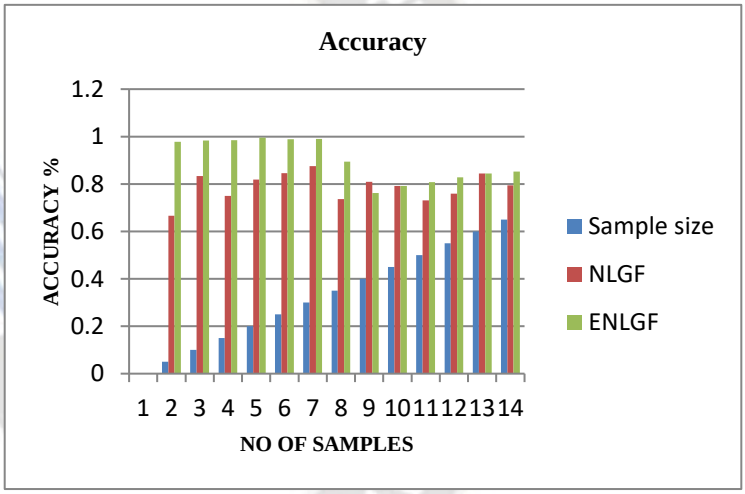

Graph 2

RF- Reg:

Sample size	NLGF	ENLGF
0.05	0.66	0.7666
0.10	0.870	0.90
0.15	0.745	0.75
0.20	0.6090	0.7272
0.25	0.690	0.76153
0.30	0.775	0.8875
0.35	0.7947	0.8894
0.40	0.7142	0.7619
0.45	0.775	0.825
0.50	0.7846	0.8076
0.55	0.6620	0.6551
0.60	0.7437	0.8562
0.65	0.4235	0.5882

Table 3: Accuracy of Random Forest Classifier

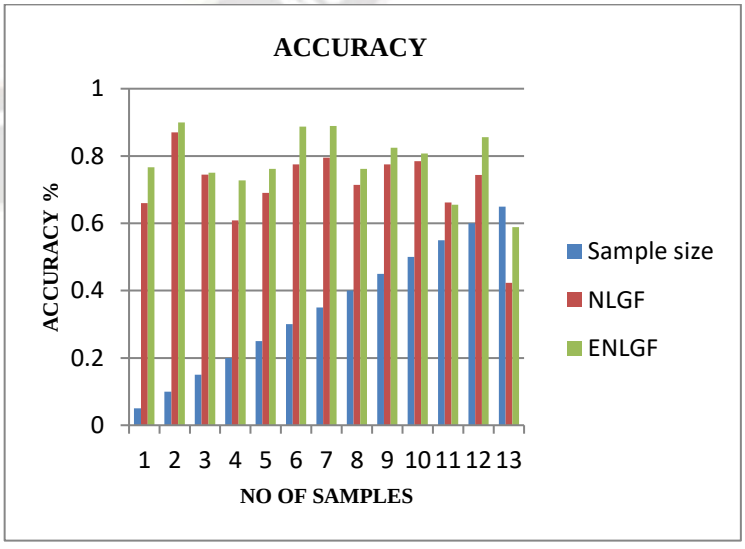

Graph 3

International Journal on Recent and Innovation Trends in Computing and Communication
ISSN: 2321-8169 Volume: 11 Issue: 7s
DOI: https://doi.org/10.17762/ijritcc.v11i7s.7021
***Article Received**: 02 April 2023 **Revised:** 24 May 2023 **Accepted:** 09 June 2023*

K MEANS:

Table 4: Accuracy of K-Means Classifier

Sample size	NLGF	ENLGF
0.05	0.01	0.02
0.10	0.0	0.0
0.15	0.0	0.0
0.20	0.0909	0.0909
0.25	0.0769	0.07692
0.30	0.0	0.0625
0.35	0.1263	0.3736
0.40	0.0	0.0476
0.45	0.0	0.0416
0.50	0.0384	0.0384
0.55	0.0172	0.0344
0.60	0.1687	0.36875
0.65	0.0294	0.0294

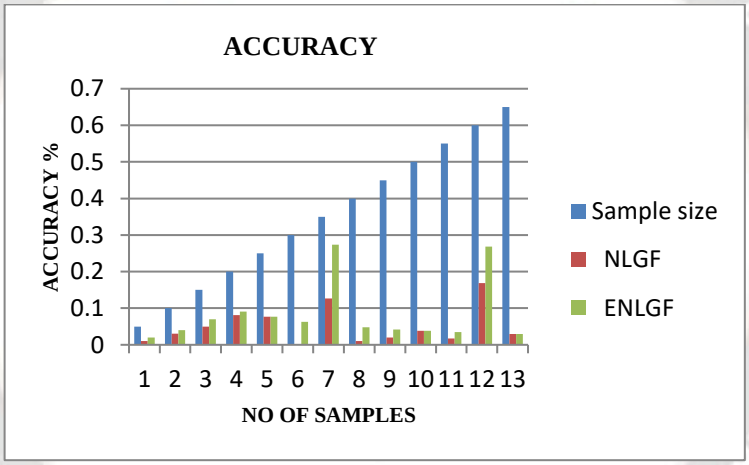

Graph 4

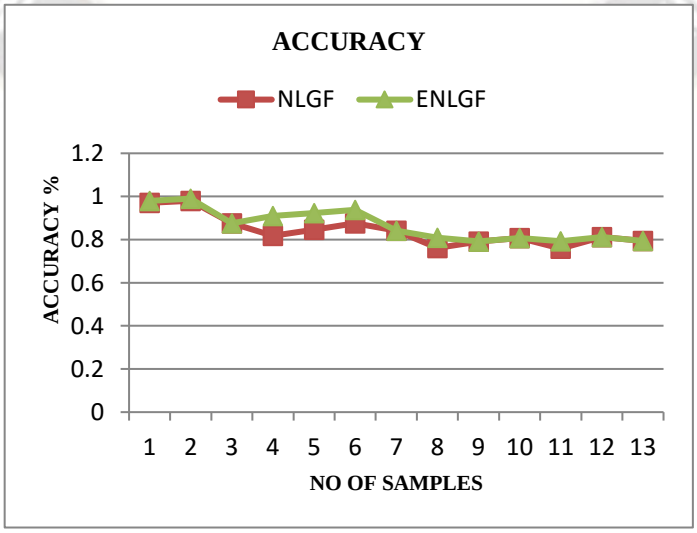

Graph 5: accuracy of SVM for NLGF and ENLGF method

International Journal on Recent and Innovation Trends in Computing and Communication
ISSN: 2321-8169 Volume: 11 Issue: 7s
DOI: https://doi.org/10.17762/ijritcc.v11i7s.7021
***Article Received**: 02 April 2023 **Revised:** 24 May 2023 **Accepted:** 09 June 2023*

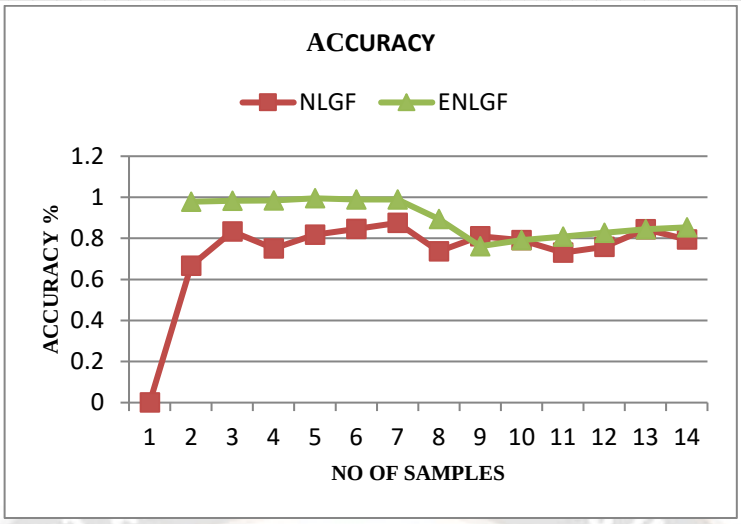

Graph 6: accuracy of LR for NLGF and ENLGF method

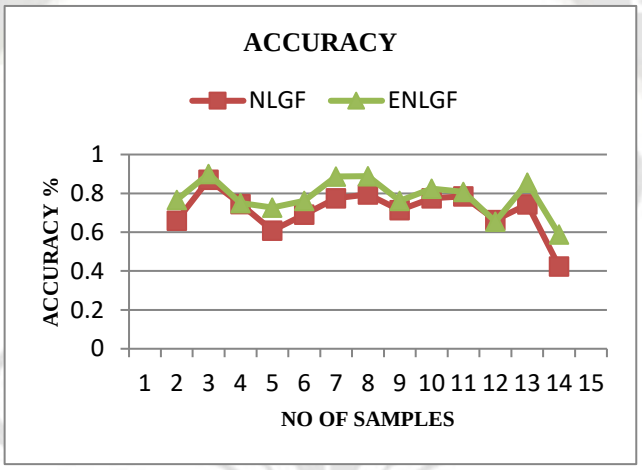

Graph 7: accuracy of RF for NLGF and ENLGF method

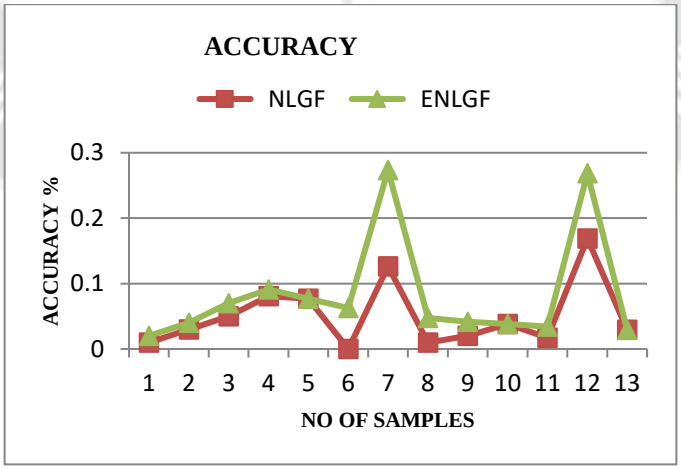

Graph 8:accuracy of K MEANS For NLGF and ENLGF

International Journal on Recent and Innovation Trends in Computing and Communication
ISSN: 2321-8169 Volume: 11 Issue: 7s
DOI: https://doi.org/10.17762/ijritcc.v11i7s.7021
***Article Received**: 02 April 2023 **Revised:** 24 May 2023 **Accepted:** 09 June 2023*

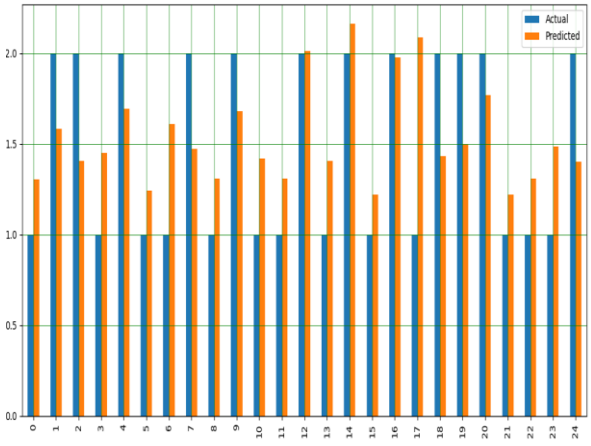

Fig: Actual and Predicted values of NLGF method

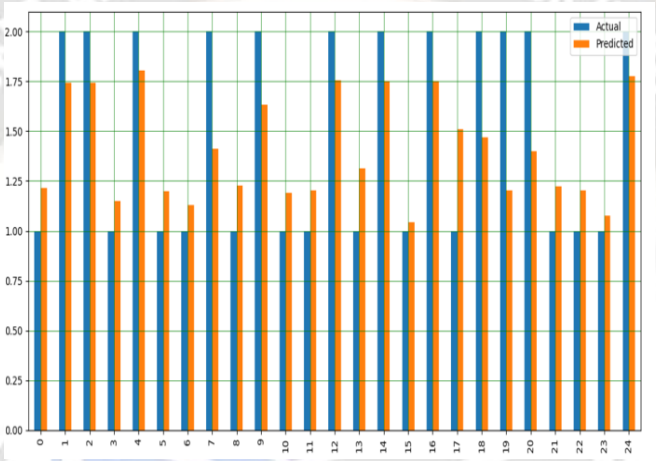

Fig: Actual and Predicted values of ENLGF method

Newton's Law of Gravitational Force (NLGF):

ACCURACY

Table 5: accuracy of different classifiers for NLGF method

Sample size	SVM	LR	DTC	RF-Regression	KNN	K MEANS
0.05	1.0	0.6666	1.0	1.0	1.0	0.01
0.10	1.0	0.8333	0.8333	1.0	1.0	0.0
0.15	0.875	0.75	0.75	1.0	1.0	0.0
0.20	0.8181	0.8181	0.8181	0.9090	0.9090	0.0909
0.25	0.8461	0.8461	0.8461	1.0	0.9230	0.0769
0.30	0.875	0.875	0.8125	0.875	0.875	0.0
0.35	0.8421	0.7368	0.8947	0.8947	0.8421`	0.1263
0.40	0.7619	0.8095	0.8095	0.7142	0.5714	0.0
0.45	0.7916	0.7916	0.875	0.875	0.625	0.0
0.50	0.8076	0.7307	0.9230	0.8846	0.6153	0.0384
0.55	0.75862	0.75862	0.9310	0.8620	0.7586	0.0172
0.60	0.8125	0.8437	0.9062	0.8437	0.78125	0.1687
0.65	0.7941	0.7941	0.8823	0.8235	0.6470	0.0294

International Journal on Recent and Innovation Trends in Computing and Communication
ISSN: 2321-8169 Volume: 11 Issue: 7s
DOI: https://doi.org/10.17762/ijritcc.v11i7s.7021
***Article Received**: 02 April 2023 **Revised:** 24 May 2023 **Accepted:** 09 June 2023*

Sample size	SVM	LR	DTC	RF-Regression	KNN
0.05	1	0.5	1	1	1
0.1	1	0.75	0.75	1	1
0.15	0.8	0.6666	0.75	1	1
0.2	0.75	0.75	0.8333	0.8571	1
0.25	0.7777	0.7777	0.8571	1	1
0.3	0.8181	0.8181	0.8	0.8181	0.8888
0.35	0.7692	0.7272	0.9	0.9	0.8888
0.4	0.6666	0.75	0.8	0.6666	0.5333
0.45	0.7222	0.7857	0.8571	0.9166	0.6111
0.5	0.7222	0.6875	0.923	0.8571	0.5789
0.55	0.7368	0.7647	0.9375	0.875	0.8
0.6	0.75	0.86666	0.8823	0.86666	0.8
0.65	0.7142	0.7647	0.8333	0.7777	0.5833

RECALL MEAN SQUARE ERROR:

Table 7: Recall of different classifiers for NLGF method

Sample size	SVM	LR	DTC	RF-Regression	KNN
0.05	1	1	1	1	1
0.1	1	0.75	0.75	1	1
0.15	1	1	0.75	1	1
0.2	1	1	0.8333	1	0.8333
0.25	1	1	0.85714	1	0.8571
0.3	1	1	0.8888	1	0.8888
0.35	1	0.8	0.9	0.9	0.8
0.4	1	0.9	0.8	0.8	0.8
0.45	1	0.8461	0.923	0.8461	0.8461
0.5	1	0.8461	0.923	0.923	0.8461
0.55	0.875	0.8125	0.9375	0.875	0.75
0.6	0.9375	0.8125	0.9375	0.8125	0.75
0.65	0.9375	0.8125	0.9375	0.875	0.875

Table 8: Mean square Error for NLGF Method

Sample size	SVM	LR	DTC	RF-Regression	KNN
0.05	0	0.3333	0	0	0
0.1	0	0.16666	0.16666	0	0
0.15	0.125	0.25	0.25	0	0
0.2	0.18181	0.18181	0.1818	0.0909	0.0909

International Journal on Recent and Innovation Trends in Computing and Communication
ISSN: 2321-8169 Volume: 11 Issue: 7s
DOI: https://doi.org/10.17762/ijritcc.v11i7s.7021
***Article Received**: 02 April 2023 **Revised:** 24 May 2023 **Accepted:** 09 June 2023*

0.25	0.1538	0.1538	0.15384	0	0.07692
0.3	0.125	0.125	0.1875	0.125	0.125
0.35	0.1578	0.2631	0.1052	0.1052	0.15789
0.4	0.238	0.1904	0.1904	0.2857	0.4285
0.45	0.2083	0.2083	0.125	0.125	0.375
0.5	0.1923	0.2692	0.07692	0.1153	0.38461
0.55	0.2413	0.2413	0.0689	0.1379	0.2413
0.6	0.1875	0.15625	0.09375	0.15625	0.21875
0.65	0.2058	0.2058	0.1176	0.1764	0.3529

MEAN ABSOLUTE ERROR: RMSE:

Table 9: Mean Absolute Error for NLGF Method

Sample size	SVM	LR	DTC	RF-Regression	KNN
0.05	0	0.3333	0	0	0
0.1	0	0.16666	0.16666	0	0
0.15	0.125	0.25	0.25	0	0
0.2	0.18181	0.18181	0.1818	0.0909	0.0909
0.25	0.1538	0.1538	0.15384	0	0.07692
0.3	0.125	0.125	0.1875	0.125	0.125
0.35	0.1578	0.2631	0.1052	0.1052	0.15789
0.4	0.238	0.1904	0.1904	0.2857	0.4285
0.45	0.2083	0.2083	0.125	0.125	0.375
0.5	0.1923	0.2692	0.07692	0.1153	0.38461
0.55	0.2413	0.2413	0.0689	0.1379	0.2413
0.6	0.1875	0.15625	0.09375	0.15625	0.21875
0.65	0.2058	0.2058	0.1176	0.1764	0.3529

Table 10: Root Mean square Error for NLGF Method

Sample size	SVM	LR	DTC	RF-Regression	KNN
0.05	0	0.5773	0	0	0
0.1	0	0.4082	0.4082	0	0
0.15	0.3535	0.75	0.5	0	0
0.2	0.4264	0.4264	0.4264	0.3015	0.3015
0.25	0.3922	0.3922	0.3922	0	0.2773
0.3	0.3535	0.3535	0.433	0.3535	0.3535
0.35	0.3973	0.5129	0.3244	0.3244	0.3973
0.4	0.4879	0.4364	0.4364	0.53452	0.6546
0.45	0.4564	0.4564	0.3535	0.3535	0.6123
0.5	0.4385	0.5188	0.2773	0.3396	0.62017

International Journal on Recent and Innovation Trends in Computing and Communication
ISSN: 2321-8169 Volume: 11 Issue: 7s
DOI: https://doi.org/10.17762/ijritcc.v11i7s.7021
***Article Received**: 02 April 2023 **Revised:** 24 May 2023 **Accepted:** 09 June 2023*

0.55	0.4913	0.4913	0.2626	0.3713	0.4913
0.6	0.433	0.3952	0.3061	0.3952	0.4677
0.65	0.4537	0.4537	0.3429	0.42	0.594

Extended Newton's Law of Gravitational Force ENLGF:

ACCURACY: PRECISION

Table11: Accuracy of ENLGF Method

Sample size	SVM	LR	DTC	RF-Regression	KNN	K MEANS
0.05	1	1	1	0.6666	0.6666	0.02
0.1	1	1	0.8333	1	0.8333	0
0.15	0.875	1	0.375	0.75	0.625	0
0.2	0.909	1	0.3636	0.7272	0.5454	0.0909
0.25	0.923	1	0.5384	0.46153	0.3076	0.07692
0.3	0.9375	1	0.6875	0.6875	0.25	0.0625
0.35	0.8421	0.8947	0.6315	0.7894	0.2631	0.3736
0.4	0.8095	0.7619	0.619	0.7619	0.3809	0.0476
0.45	0.7916	0.7916	0.625	0.625	0.375	0.0416
0.5	0.8076	0.8076	0.6538	0.8076	0.423	0.0384
0.55	0.7931	0.8275	0.6206	0.6551	0.4482	0.0344
0.6	0.8125	0.84375	0.5312	0.6562	0.4375	0.36875
0.65	0.7941	0.8529	0.5588	0.5882	0.5882	0.0294
0.7	0.7837	0.6486	0.5945	0.5945	0.6486	0.027
0.75	0.7948	0.7692	0.5897	0.5897	0.5897	0.0256

Table 12 : Precision of ENLGF Method

Sample size	SVM	LR	DTC	RF-Regression	KNN
0.05	1	1	1	1	1
0.1	1	1	0.75	1	0.75
0.15	0.8	1	0.4	0.66666	0.6
0.2	0.8571	1	0.3333	0.8	0.5714
0.25	0.875	1	0.6666	0.5	0.25
0.3	0.9	1	0.6666	0.7	0.2
0.35	0.8181	0.9	0.6666	0.875	0.16666
0.4	0.7142	0.6923	0.5625	0.6923	0.3333
0.45	0.75	0.75	0.625	0.6666	0.25
0.5	0.75	0.75	0.6428	0.7222	0.375
0.55	0.7777	0.8235	0.7777	0.8	0
0.6	0.7777	0.8235	0.5384	0.7272	0.4166
0.65	0.7368	0.8235	0.5294	0.5454	0.5416
0.7	0.75	0.6666	0.5789	0.5652	0.6315
0.75	0.7619	0.75	0.5714	0.5652	0.5555

International Journal on Recent and Innovation Trends in Computing and Communication
ISSN: 2321-8169 Volume: 11 Issue: 7s
DOI: https://doi.org/10.17762/ijritcc.v11i7s.7021
***Article Received**: 02 April 2023 **Revised:** 24 May 2023 **Accepted:** 09 June 2023*

RECALL:

MEAN ABSOLUTE ERROR:

Table 13: Recall For ENLGF

Sample size	SVM	LR	DTC	RF-Regression	KNN
0.05	1	1	1	1	1
0.1	1	1	1	1	1
0.15	1	1	0.5	1	0.75
0.2	1	1	0.1666	0.66666	0.66666
0.25	1	1	0.2857	0.4285	0.1428
0.3	1	1	0.8888	0.7777	0.1111
0.35	1	0.9	0.6	0.7	0.1
0.4	1	0.9	0.9	0.9	0.3
0.45	0.923	0.923	0.7692	0.6153	0.0769
0.5	0.923	0.923	0.6923	1	0.2307
0.55	0.875	0.875	0.4375	0.5	0
0.6	0.875	0.875	0.4375	0.5	0.3125
0.65	0.875	0.875	0.5625	0.75	0.8125
0.7	0.8333	0.5555	0.6111	0.7222	0.6666
0.75	0.8421	0.7894	0.6315	0.6842	0.7894

Table 14: Mean Absolute Error For ENLGF

Sample size	SVM	LR	DTC	RF-Regression	KNN
0.05	0	0	0	0.3333	0.3333
0.1	0	0	0.1666	0	0.1666
0.15	0.125	0	0.625	0.25	0.375
0.2	0.0909	0	0.6363	0.2727	0.4545
0.25	0.0769	0	0.4615	0.5384	0.6923
0.3	0.0625	0	0.3125	0.3125	0.75
0.35	0.1578	0.1052	0.3684	0.2105	0.7368
0.4	0.1904	0.238	0.3809	0.238	0.619
0.45	0.2083	0.2083	0.375	0.375	0.625
0.5	0.1923	0.1923	0.3461	0.1923	0.5769
0.55	0.2068	0.1724	0.3793	0.3448	0.5517
0.6	0.1875	0.1562	0.4687	0.3437	0.5625
0.65	0.2058	0.147	0.4411	0.4117	0.4117
0.7	0.2162	0.3513	0.4054	0.4054	0.3513
0.75	0.2051	0.2307	0.4102	0.4102	0.4102

MEAN SQUARE ERROR

International Journal on Recent and Innovation Trends in Computing and Communication
ISSN: 2321-8169 Volume: 11 Issue: 7s
DOI: https://doi.org/10.17762/ijritcc.v11i7s.7021
***Article Received**: 02 April 2023 **Revised:** 24 May 2023 **Accepted:** 09 June 2023*

ROOT MEAN SQUARE ERROR:

Sample size	SVM	LR	DTC	RF-Regression	KNN
0.05	0	0	0	0.3333	0.3333
0.1	0	0	0.1666	0	0.1666
0.15	0.125	0	0.625	0.25	0.375
0.2	0.0909	0	0.6363	0.2727	0.4545
0.25	0.0769	0	0.4615	0.5384	0.6923
0.3	0.0625	0	0.3125	0.3125	0.75
0.35	0.1578	0.1052	0.3684	0.2105	0.7368
0.4	0.1904	0.238	0.3809	0.238	0.619
0.45	0.2083	0.2083	0.375	0.375	0.625
0.5	0.1923	0.1923	0.3461	0.1923	0.5769
0.55	0.2068	0.1724	0.3793	0.3448	0.5517
0.6	0.1875	0.15625	0.46875	0.34375	0.5625
0.65	0.2058	0.147	0.4411	0.4117	0.4117
0.7	0.2162	0.3513	0.4054	0.4054	0.3513
0.75	0.2051	0.2307	0.4102	0.4102	0.4102

Sample size	SVM	LR	DTC	RF-Regression	KNN
0.05	0	0	0	0.5773	0.5773
0.1	0	0	0.4082	0	0.4082
0.15	0.3535	0	0.7905	0.5	0.6123
0.2	0.3015	0	0.7977	0.5222	0.6741
0.25	0.2773	0	0.6793	0.7337	0.832
0.3	0.25	0	0.559	0.559	0.866
0.35	0.3973	0.3244	0.6069	0.4588	0.8583
0.4	0.4364	0.4879	0.6172	0.4879	0.7867
0.45	0.4564	0.4564	0.6123	0.6123	0.7905
0.5	0.4385	0.4385	0.5883	0.4385	0.7595
0.55	0.4548	0.4152	0.6158	0.5872	0.7427
0.6	0.433	0.3952	0.6846	0.5863	0.75
0.65	0.4537	0.3834	0.6642	0.6416	0.6416
0.7	0.4649	0.5927	0.6367	0.6367	0.5927
0.75	0.4529	0.4803	0.6405	0.6405	0.6405

VII. CONCLUSIONS

One of the difficult research ideas in machine learning technologies is face recognition. In this research, new machine learning methods are suggested that use Newton's third law of gravitational force and angel to find relationships between pixels and pixels. The differences in illumination, rotation invariance, and noisy face pictures are taken care of by the amount and direction of the local gravitational force. For classification, many machine learning classifiers are employed., and it has been discussed how accurate each classifier is. Overall, I can say that

International Journal on Recent and Innovation Trends in Computing and Communication
ISSN: 2321-8169 Volume: 11 Issue: 7s
DOI: https://doi.org/10.17762/ijritcc.v11i7s.7021
***Article Received**: 02 April 2023 **Revised:** 24 May 2023 **Accepted:** 09 June 2023*

the suggested NLGF approach accurately and efficiently detects faces in photos with little computational cost. The identification of video images will be done in the future using the same approach.

REFERENCES

[1] B. Moghaddam, T. Jebara, and A. Petland, "Bayesian face recognition," J. Pattern Recognit., vol. 33, no. 11, pp. 1771–1782, 2000.

[2] G. Guo, S. Li, and K. Chan, "Face recognition by support vector machines," in Proc. IEEE International Conference on Automatic Face and Gesture Recognition (AFGR'00), 2000, pp. 196–201

[3] M. Turk and A. Pentland, "Eigen faces for recognition," J. Cognitive Neursci., vol. 3, no. 1, pp. 71–86, 1991.

[4] R.C.Gonzalez and R. E. Woods, Digital Image Processing. Pearson Prentice Hall, 3rd Edition.

[5] M. Savvides and V. Kumar, "Illumination normalization using logarithm transforms for face authentication," in Proc. IAPR AVBPA, 2003, pp.549–556.

[6] S.M.Pizerand E. P. Amburn, "Adaptive histogram equalization and its variations," J. Comput. Vis. Graph. Image Process., vol. 39, no. 3, pp. 355–368, 1987.

[7] V. Blanz and T. Vetter, "Face recognition based on fitting a 3d morphable model," IEEE Trans. Pattern Anal. Mach. Intell., vol. 25, no. 9, pp.1063–1073, 2003

[8] L. Zheng, Y. Yang, and Q. Tian, "Sift meets cnn: A decade survey of instance retrieval," arXiv reprint arXiv:1608.01807v2, 2015.

[9] Fan, B., Kong, Q., Trzcinski, T., Wang, Z., Pan, C., &Fua, P. (2014). Receptive fields selection for binary feature description. IEEE Transactions on Image Processing, 26(6), 2583–2595.

[10] Trzcinski, T., Christoudias, M., Lepetit, V., &Fua, P. (2012). Learning image descriptors with the boosting-trick. In Advances in neural information processing systems (pp. 269–277).

[11] Balntas, V., Tang, L., &Mikolajczyk, K. (2015). Bold - binary online learned descriptor for efficient image matching. In Proceedings of the IEEE conference on computer vision and pattern recognition (CVPR) (pp. 2367–2375)

[12] D. Lowe, "Distinctive image features from scale invariant key points," Int. J. Comput. Vis., vol. 60, no. 2, pp. 91–110, 2004.

[13] H. Bay, A. Ess, T. Tuytelaars, and L. V. Gool, "Speeded-up robust features (surf)," J. omput. Vis. Img. Understanding, vol. 110, no. 3,pp. 346–359, 2008.

[14] E. Tola, V. Lepetit, and P. Fua, "Daisy: An efficient dense descriptor applied to wide-baseline stereo," IEEE Trans. Pattern Anal. Mach. Intell., vol. 32, no. 5, pp. 815–830, 2010.

[15] A. Iscen, G. Tolias, P. Gosselin, and H. Jeguo, "A comparison of dense region detectors for image search and fine-grained classification," IEEE Trans. Image Process., vol. 24, no. 8, pp. 2369–2381, 2015.

[16] C.Nagaraju, D.Sharadamani, C.Maheswari and D.Vishnu Vardhan Evaluation of LBP-Based Facial emotions recognition techniques to make consistent decisions Int.J.Pattern Recognition AND Artificial Intelligence 2015.

[17] D.G. Lowe, "Distinctive Image Features from Scale Invariant Keypoints," Int'l J. Computer Vision, vol. 20, no. 2, pp. 91-110, 2004

[18] C. Strecha, T. Tuytelaars, and L. Van Gool, "Dense Matching of Multiple Wide Baseline Views," Proc. Int'l Conf. Computer Vision,2003.

[19] Lin, K., Lu, J., Chen, C. S., Zhou, J., & Sun, M. T. (2018). Unsupervised deep learning of compact binary descriptors. IEEE Transactions on Pattern Analysis and Machine Intelligence, 41(6), 1501–514.

[20] J Ma, X Jiang , A Fan, J Jiang, J Yan 2021 .image matching from handcrafted to deep features: A survey , International Journal of Computer Visionvolume 129, pages23–79 (2021).

[21] Dr. B. Maruthi Shankar. (2019). Neural Network Based Hurdle Avoidance System for Smart Vehicles. International Journal of New Practices in Management and Engineering, 8(04), 01 - 07. https://doi.org/10.17762/ijnpme.v8i04.79

[22] Tuytelaars, T., Mikolajczyk, K., et al. (2008). Local invariant feature detectors: A survey. Foundations and Trends® in Computer Graphics and Vision, 3(3), 177–280.

[23] Li, Y., Wang, S., Tian, Q., & Ding, X. (2015). A survey of recent advances in visual feature detection. Neurocomputing, 149, 736–751.

[24] Rosten, E., Porter, R., & Drummond, T. (2010). Faster and better: A machine learning approach to corner detection. IEEE Transactions on Pattern Analysis and Machine Intelligence, 32(1), 105–119.

[25] Moravec, H. P. (1977). Techniques towards automatic visual obstacle avoidance.

[26] Smith, S. M., & Brady, J. M. (1997). Susan: A new approach to low level image processing. International Journal of Computer Vision, 23(1), 45–78.

[27] Belongie, S., Malik, J., &Puzicha, J. (2002). Shape matching and object recognition using shape contexts. IEEE Transactions on Pattern Analysis and Machine Intelligence, 4, 509–522.

[28] Richardson, A., & Olson, E. (2013). Learning convolutional filters for interest point detection. In Proceedings of the IEEE international conference on robotics and automation, pp. 631–637.

[29] Parjane, V. A. ., Arjariya, T. ., & Gangwar, M. . (2023). Corrosion Detection and Prediction for Underwater pipelines using IoT and Machine Learning Techniques. International Journal of Intelligent Systems and Applications in Engineering, 11(2s), 293 –. Retrieved from https://ijisae.org/index.php/IJISAE/article/view/2626

[30] Strecha, C., Lindner, A., Ali, K., &Fua, P. (2009). Training for task specific keypoint detection. In Joint pattern recognition symposium, Springer, pp. 151–160.

[31] Trajković, M., & Hedley, M. (1998). Fast corner detection. Image and Vision Computing, 16(2), 75–87.

[32] Zhang, X., Yu, F. X., Karaman, S., & Chang, S. F. (2017b). Learning discriminative and transformation covariant local

International Journal on Recent and Innovation Trends in Computing and Communication
ISSN: 2321-8169 Volume: 11 Issue: 7s
DOI: https://doi.org/10.17762/ijritcc.v11i7s.7021
***Article Received**: 02 April 2023 **Revised:** 24 May 2023 **Accepted:** 09 June 2023*

feature detectors. In Proceedings of the IEEE conference on computer vision and pattern recognition, pp. 6818–6826.

[33] Prateek Singhal, Prabhat Kumar Srivastava., Arvind Kumar Tiwari, Ratnesh Kumar Shukla **"**A Survey: Approaches to Facial Detection and Recognition with Machine Learning Techniques". Proceedings of Second Doctoral Symposium on Computational Intelligence 2021.

[34] Mwangi, J., Cohen, D., Silva, C., Min-ji, K., & Suzuki, H. Feature Extraction Techniques for Natural Language Processing Tasks. Kuwait Journal of Machine Learning, 1(3). Retrieved from http://kuwaitjournals.com/index.php/kjml/article/view/137

[35] Bhanushree K. J., Meenavathi M. B "Feature Based Face Recognition using Machine Learning Techniques", International Journal of Recent Technology and Engineering (IJRTE) ISSN: 2277-3878, Volume-8 Issue-6, March 2020